DTU Library

Kinematic analysis of a lightweight periodic dielectric structure of pearls for RF coaxial power cables for space applications

Kress, Gerald; Karstensen, Holger; Mattes, Michael; Raboso, David

Published in:
International Journal of Space Science and Engineering

Link to article, DOI:
10.1504/IJSPACESE.2020.10032053

Publication date:
2020

Document Version
Peer reviewed version

Citation (APA):
Kress, G., Karstensen, H., Mattes, M., & Raboso, D. (2020). Kinematic analysis of a lightweight periodic dielectric structure of pearls for RF coaxial power cables for space applications. *International Journal of Space Science and Engineering*, *6*(1), 28-48. https://doi.org/10.1504/IJSPACESE.2020.10032053

Kinematic analysis of a lightweight periodic dielectric structure of pearls for RF coaxial power cables for space applications

Gerald Kress

Composite Materials and Adaptive Structures, Department of Mechanical and Process Engineering,
ETH Zürich,
CH-8092 Zürich, Zürich, Switzerland
Fax: +41446321338 E-mail: gkress@ethz.ch

Holger Karstensen

Dr.-Ing. Karstensen Consulting,
Hubertusstr. 2,
D-85662 Hohenbrunn, Bavaria, Germany
Fax: +49 8102 748526 E-mail: holger@karstensen.biz

Michael Mattes

Department of Electrical Engineering,
Technical University of Denmark,
Ørstedts Plads 348
DK-2800 Kgd. Lyngby, Denmark
Fax: +49 8102 748526 E-mail: mmattes@elektro.dtu.dk

David Raboso

European Space Agency,
Universidad Politécnica Valencia,
Camino de Vera s/n, CPI (Edificio 8G - Acceso B - Planta B),
46022 Valencia, Spain
Fax: +43(96) 2051402 E-mail: david.raboso@esa.int

Abstract: The desire to reduce the mass per unit length and to increase phase stability of coaxial radio-frequency (RF) power cables for space application motivates to replace solid dielectric with a periodic chain of hollow pearls. The design of the dielectric pearls must allow for bending flexibility of the cable even if they are made from a stiff material such as silicon glass. An important requirement of RF power cables for space applications is their phase stability, which is influenced by the material-dielectric-constant tolerance over a large temperature range as well as by changes in geometry. This paper presents a closed-form model based on rigid-body motion to predict the kinematic response of dielectric pearls to the bending of the cable. Particularly, the model maps the eccentricity of the inner and outer conductors with respect to each other and the axial strain of the bent cable along its centerline.

Keywords: Dielectric; Co-Axial RF Power Cable; Space Applications; Kinematics; Closed-Form Modeling.

Reference ‘Kinematic analysis of a lightweight periodic dielectric structure of pearls for RF coaxial power cables for space applications’, *International Journal of Space Science and Engineering*, Vol. x, No. x, pp.xxx–xxx.

1 Introduction

1.1 Coaxial RF cables for space applications

The typical coaxial cable consists of an inner conductor surrounded by a tubular insulation layer, called dielectric, that in turn is surrounded by a conducting shield. The primary task of the dielectric is to hold the inner conductor in place with respect to the outer one. In vacuum or near-vacuum conditions radio-frequency fields can accelerate electrons resulting in an electron avalanche caused by secondary electron emission. This phenomenon is known as multipactor effect [1]. For space application, where multipactor is a critical issue, the dielectric material or structure must separate inner and outer conductors so that no gaps exist. Typical state-of-the-art cables use a solid dielectric made from PTFE [2], which undergoes a structural phase change at $20^\circ C$ that causes a nonlinear phase change with temperature due to the changing dielectric constant. Earlier attempts of reducing weight by e.g. reducing the mass of the dielectric (foamed or sintered material with large amount of air in the volume) led to lower mechanical stability and impaired phase linearity. Moreover, when operating cables at high power levels the temperature inside the cable becomes high. This high temperature, together with a high thermal-expansion mismatch between the dielectric and the conductors, causes undesired phase shifts of the electrical signal and, consequently, significant distortion of the signal quality. Better heat evacuation is an advantage of dielectric structures over solid or foamed dielectrics, and earlier design suggestions for dielectric structures can be found in the handbook by Spergel [3].

1.2 Summary of present work

The present work responds to the necessity of being able to predict the eccentricity between the inner and outer conductors which is caused by bending of the coaxial cable where the periodic dielectric structure indicated in Fig. 1 is formed by a chain of spherical bodies named SucoPearls by [4]. It focuses on the development of an analytical model which is based on kinematic considerations, the verification of the model, and the presentation of its results on the industrial designs SP304 and SP306 developed by Karstensen et al. [5, 6].

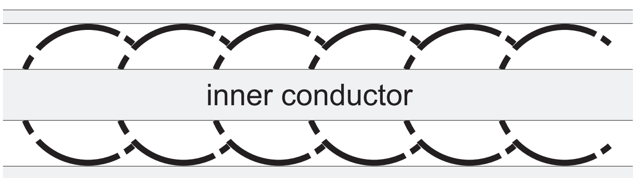

Figure 1 SucoPearl dielectric geometric design principle (with venting holes indicated)

The mental picture leading to the model is that the inner conductor is bent to a perfectly circular shape and that the periodically arranged SucoPearls undergo rigid body motions as they adapt to the new positions on the bent inner conductor under the constraints imposed by the interactions with adjacent SucoPearls.
The model assumptions are justifiable if the inner conductor is much stiffer than all other cable components, and the SucoPearls are much stiffer than the components of which the outer parts of the cable are made. The conditions are closely approximated if the inner conductor tube is made from solid Invar® steel and the outer conductor is made from wound copper band and the shield jacket from aluminum weave, which is the current design.

1.3 Paper structure

Section 2 *Geometry* defines the SucoPearl shape parameters as well as the periodic structure formed by the chain of SucoPearls. The description of shape and periodicity immediately yields formulas for volume fraction with respect to the volume consumed by a solid-dielectric, and the corresponding mass fractions. Section 3 *bending kinematics* develops a closed-form model that predicts relative SucoPearl rotations limited by the constraint that gaps must not occur, eccentricity of inner and outer conductors with respect to each other, axial SucoPearl stretching, and contacting ring elongation, all due to bending. Section 4 *Results for relevant geometries and bending* is dedicated to the two sample cable designs SP304 and SP306 developed by Huber+Suhner [4]. The systematic eccentricity imminent to the SucoPearl design is compared to an estimate of eccentricity occurring in solid PTFE dielectric designs in Section 5 *Critical discussion.* Section 6 *Conclusion and outlook* is followed by a list of symbols.

2 Geometry

2.1 Parameters, periodic length, and volume fraction

Fig. 2 presents the parameterization scheme of the SucoPearls. The wall thickness is assumed to be constant over the whole spherical domain. The mean radius of the SucoPearl is

$$r_M = \frac{1}{2}\left(r_I + r_O\right) \ . \tag{1}$$

Two cut-outs bound the spherical domain: There is the necessity to allow the inner conductor with radius r_{IC} to pass through the SucoPearls, and there is also the necessity to allow two adjacent SucoPearls to interact with each other in a kinematically defined way. The spacing between any two adjacent SucoPearls, or the periodic-structure unit-cell length, Δ_{SP} follows from the

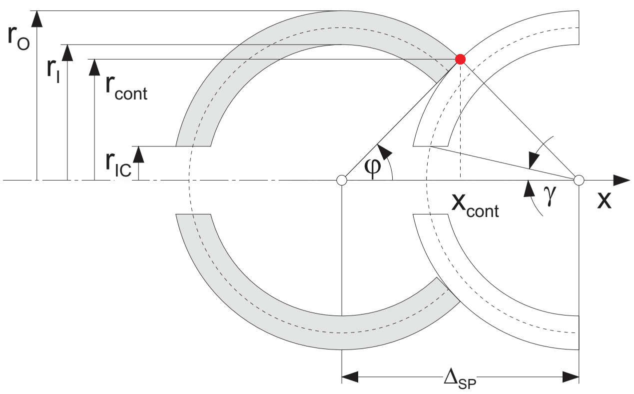

Figure 2 SucoPearl geometry parameters

condition that the SucoPearl to the right contacts the opening of the adjacent SucoPearl to the left at the point

$$x_{cont} = r_O \, cos\varphi \qquad r_{cont} = r_O \, sin\varphi \, . \tag{2}$$

The sketches in Fig. 3 suggest that the surfaces of the openings be manufactured so that the open contacting

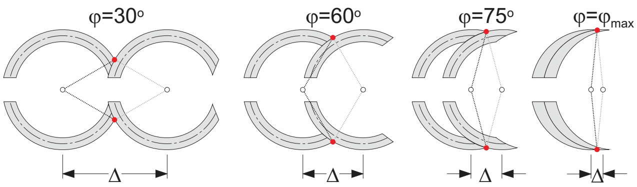

Figure 3 Adjacent SucoPearls for various opening angles

surfaces take spherical shapes. Figs. 2 and 3 illustrate that the choice of contacting points being located at the outer surface on both sides of each sphere gives the spacing of sphere centers Δ_{SP}:

$$\Delta_{SP} = 2 r_O \, cos\varphi \, ; \quad 0 \le \varphi < \varphi_{max} \, , \tag{3}$$

where the upper bound φ_{max} follows from the constraint that adjacent spheres, at $r = 0$, must not penetrate themselves:

$$2 r_O \, cos\varphi \ge r_O - r_I \;\Rightarrow\; \varphi_{max} = acos\left(\frac{r_O - r_I}{2 r_O}\right) \, . \tag{4}$$

Each individual SucoPearl occupies a length L_{SP}:

$$L_{SP} = (1 + cos\varphi) \, r_O \, ; \quad 0 \le \varphi < \varphi_{max} \, . \tag{5}$$

As the SucoPearls repeat themselves with periodicity Δ_{SP}, and each one has a length L_{SP}, the real number of spheres within one unit cell of length Δ_{SP} is given by:

$$N_{SP} = \frac{1 + cos\varphi}{2 cos\varphi} \, . \tag{6}$$

When the spheres are closest to each other, $\varphi = \varphi_{max}$, N_{SP} becomes:

$$N_{SP} \left(\varphi_{max}\right) = \frac{3 r_O - r_I}{2 r_O - 2 r_I} \, . \tag{7}$$

For a solid sphere, $r_I = 0$, $\varphi_{max} = 60°$ and $N_{sphere} = \frac{3}{2}$.

2.2 Volume fraction

Within the length L_{SP} of one SucoPearl, a compact solid dielectric would form a cylinder of volume V_{cyl}:

$$V_{cyl} = \pi \left(r_O^2 - r_{IC}^2\right) L_{SP} \tag{8}$$

The same length is populated by N_s SucoPearls each of which has a volume of V_{SP}, so that the volume fraction follows from

$$v_f = \frac{V_{SP}}{V_{cyl}} N_{SP} \, . \tag{9}$$

Fig. 4 shows a SucoPearl to the left whose opening shape at its right fits the spherical outer surface of its neighbor to the right. The curved triangle whose vertexes are marked with solid circles follows from subtracting the intersecting areas of the two adjacent SucoPearls. The

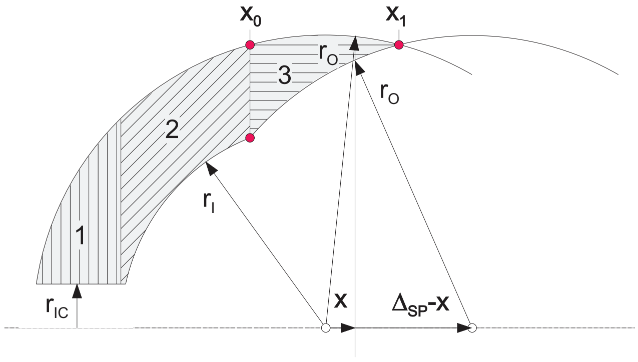

Figure 4 Calculation of the volume of one SucoPearl

axial coordinates of the vertexes are given by:

$$x_0 = \frac{\Delta_{SP}}{2} - \frac{r_O^2 - r_I^2}{2 \Delta_{SP}} \, ; \quad x_1 = r_O \, cos\varphi \, . \tag{10}$$

The resulting net volume of the incomplete SucoPearl can be calculated by the method of integrating infinitesimal slices of the three different regions:

$$V_{SP} = V_1 + V_2 + V_3$$

$$\begin{aligned}
V_1 &= \pi \int_{-r_O}^{-r_I} \left(r_O^2 - x^2\right) dx \\
V_2 &= \pi \int_{-r_I}^{x_0} \left[\left(r_O^2 - x^2\right) - \left(r_I^2 - x^2\right)\right] dx \\
V_3 &= \pi \int_{x_0}^{x_1} \left[\left(r_O^2 - x^2\right) - \left(r_O^2 - \left(\Delta_{SP} - x\right)^2\right)\right] dx
\end{aligned} \tag{11}$$

Carrying out the integrations one obtains:

$$\begin{aligned}
V_1 &= \frac{\pi}{3}\left(2 r_O^3 + r_I^3 - 3 r_O^2 r_I\right) \\
V_2 &= \pi \left(r_O^2 - r_I^2\right)\left(r_I + r_O \, cos\varphi - \frac{r_O^2 - r_I^2}{4 r_O \, cos\varphi}\right) \, . \\
V_3 &= \pi \frac{\left(r_O^2 - r_I^2\right)^2}{8 r_O \, cos\varphi}
\end{aligned} \tag{12}$$

The volumes of the solid cylinder (8), of the SucoPearl (11), and the volume fraction (9) are plotted versus the opening angle in Fig. 5. Whereas the volume fraction

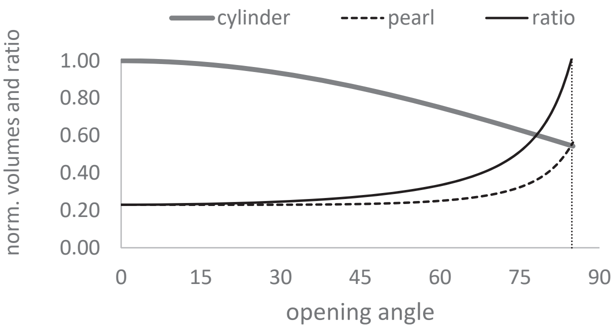

Figure 5 Normalized volumes of SucoPearls and solid cylinder, and volume fraction v_f. Data: $r_O = 1.93$, $r_I = 1.73$, $r_{IC} = 0.815$

is normalized per se, the other two volumes V_{cyl} and V_{SP} are both normalized with respect to the maximum value of $V_{cyl}(\varphi = 0)$. The cylinder volume decreases proportionally with decreasing length of one SucoPearl and the SucoPearl volume increases because the real number of SucoPearls within the length of an individual SucoPearl increases. Mass fractions per unit length are

$$m_f = \frac{\rho_{SP}\, V_{SP}}{\rho_{cyl}\, V_{cyl}} \frac{N_{SP}}{L_{SP}}\,, \tag{13}$$

where ρ_{SP} and ρ_{cyl} are the mass densities of SucoPearls and the solid-dielectric, respectively. Fig. 6 illustrates the

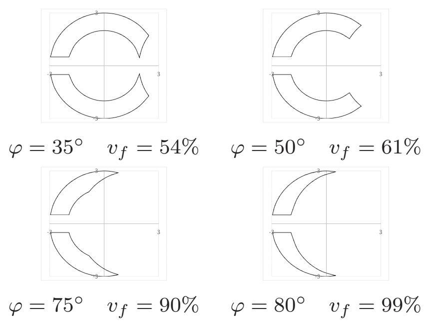

Figure 6 SucoPearl shapes and volume fractions

relation between SucoPearl opening angle and volume fraction for a SucoPearl with large sphere-shell thickness.

3 Bending kinematics

During bending action, adjacent SucoPearls slide on each other so that large rotations can be described with trigonometric relations. Because of the rotation, the SucoPearl sphere center points must be on a circle with radius R_{CP} that cannot be the same as the nominal radius R_N of the circle that is formed by the bent inner conductor. The eccentricity is kinematically coupled with axial stretch. Both effects are influenced by the position of the ring-shaped contact at which the SucoPearl contacts the inner conductor. Inherent verification of the model equations is given with the deformed-configuration plots.

3.1 Large rotation of a SucoPearl about its neighbor

Let the center line of the inner conductor be bent to a circle with nominal radius R_N. The center points C of the small holes of the SucoPearls are on that circle. Due to their a spherical contour, the ring-shaped edge of the large hole of one SucoPearl on the spherical surface of its neighbor is possible without creating a gap between the two bodies appearing, as Fig. 7 illustrates. The same figure also shows that the sliding motion of the SucoPearl with center point B, where the prime denotes deformed configuration, is simply a rotation about its neighboring SucoPearl's center point A.

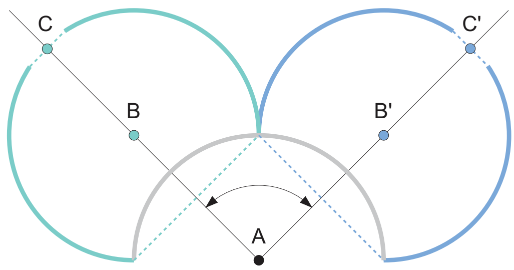

Figure 7 Sliding of a SucoPearl on its adjacent neighbor

3.2 Bending radii of inner and outer conductors

The kinematic analysis is based on the insight that the points A, B, and C must be connected by a straight line in all configurations. Because of their spherical shape, the SucoPearl center points must be on the same radius as the bent outer-conductor center line R_{CP}. Figure 8 illustrates that the two radii cannot be the same and that the radius of the inner-conductor center line must be larger than the outer-conductor centerline, or $R_N > R_{CP}$. The difference between the two radii creates the eccentricity e of the cross-sectional centers of the inner and outer conductors:

$$e = R_N - R_{CP}\,. \tag{14}$$

The objective of the following derivations is to find the radius R_{CP} as it depends on the nominal bending radius R_N and geometric parameters. The point coordinates in reference coordinates are:

$$\begin{aligned} x_A &= R_{CP} & y_A &= 0 \\ x_B &= R_{CP}\, cos\alpha_B & y_B &= R_{CP}\, sin\alpha_B\,. \\ x_C &= R_N\ \ cos\alpha_C & y_C &= R_N\ \ sin\alpha_C \end{aligned} \tag{15}$$

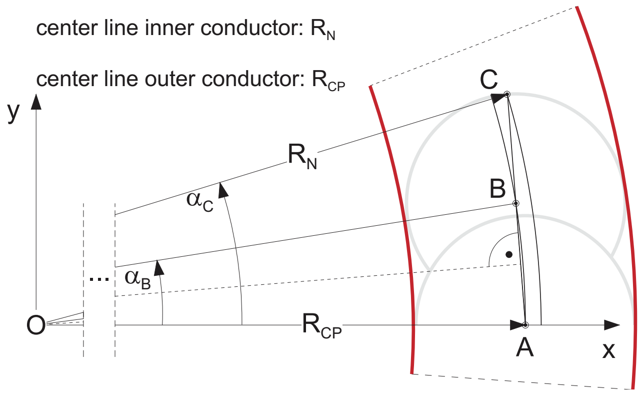

Figure 8 The sphere centers lie on a smaller radius than the inner conductor center line

If the inner conductor is made from a much stiffer material than other cable components, it may be assumed that its centerline length will not change with deformation. Therefore, the arc length of the bent centerline,

$$\alpha_C R_N = \Delta_{SP} + r_M \quad \Rightarrow \quad \alpha_C = \frac{\Delta_{SP} + r_M}{R_N}, \tag{16}$$

is a constant, which circumstance determines with the angle α_C the coordinates of point C in (15). The rotation must not be so large as to open a gap between inner and outer conductors:

$$\alpha_C \leq \alpha_{lim} = asin\left(\frac{r_{IC}}{R_O}\right). \tag{17}$$

The maximum rotation α_{lim} corresponds with a minimum nominal bending radius R_{lim}:

$$R_N \geq R_{lim} = \frac{\Delta_{SP} + r_M}{\alpha_{lim}}. \tag{18}$$

3.3 Axial stretch due to bending

As a consequence of assuming that the inner conductor's length remains constant, the straight line connecting points A, B, and C is smaller in the deformed than in the reference configurations, respectively. We assume that all other parts change length by the same global stretch λ:

$$\lambda = \frac{\overline{AC}}{R_N \alpha_C}. \tag{19}$$

A second simplifying assumption is that the radius R_{CP} on which the Sucopearl's center points lie is related to the nominal bending radius R_N by the same stretch as that of the axial direction of individual SucoPearls:

$$R_{CP} = \lambda R_N = \frac{\overline{AC}}{\alpha_C} \tag{20}$$

Both SucoPearl-center points A and B lie on the same radius R_{CP}. The dotted line in Figure 8 connects the origin $x = y = 0$ with the center of both points, is therefore perpendicular to the line connecting the points A and B, and bisects the angle α_B. This allows connecting the latter with the distance between points A and B:

$$\begin{aligned} \Delta_{SP} - \Delta L &= 2R_{CP} sin\left(\tfrac{1}{2}\alpha_B\right) \\ \Rightarrow sin\left(\tfrac{1}{2}\alpha_B\right) &= \frac{\Delta_{SP}\lambda}{2R_{CP}} = \frac{\Delta_{SP}}{2R_N} = K \cdot \\ \Rightarrow cos\left(\tfrac{1}{2}\alpha_B\right) &= \sqrt{1-K^2} \end{aligned} \tag{21}$$

The trigonometric functions of the half angle are related to those of the full angle by:

$$\begin{aligned} sin\left(\alpha_B\right) &= 2sin\left(\tfrac{1}{2}\alpha_B\right)cos\left(\tfrac{1}{2}\alpha_B\right) \\ &= 2K\sqrt{1-K^2} \\ cos\left(\alpha_B\right) &= cos^2\left(\tfrac{1}{2}\alpha_B\right) - sin^2\left(\tfrac{1}{2}\alpha_B\right) \cdot \\ &= 1 - K^2 - K^2 \\ &= 1 - 2K^2 \end{aligned} \tag{22}$$

The radius R_{CP} is determined by the requirement that points A, B, and C must be on a straight line which is expressed by the rule of proportion:

$$\begin{aligned} \left(y_C - y_A\right)\left(x_B - x_A\right) &= \left(y_B - y_A\right)\left(x_C - x_A\right) \\ y_C\left(x_B - x_A\right) &= \quad y_B\left(x_C - x_A\right) \\ y_C\left(cos\alpha_B - 1\right) &= \quad sin\alpha_B\left(x_C - R_{CP}\right) \\ R_{CP} &= \quad x_C + \frac{1 - cos\alpha_B}{sin\alpha_B} y_C \end{aligned} \tag{23}$$

3.4 Inner-conductor contact position modeling

The SucoPearl center points lie on the radius R_{CP} (23) that is given by the closed-form expression,

$$R_{CP} = \left[cos\,\alpha_C + \frac{\Delta_{SP}}{\sqrt{4R_N^2 - \Delta_{SP}^2}} sin\,\alpha_C\right] R_N, \tag{24}$$

that depends on the SucoPearl geometric characteristics, where α_C is given by (16). Fig. 9 illustrates the kinematic model for a relatively thick-walled SucoPearl with a wide opening angle. Both plots show that adjacent SucoPearl rotate about each other so that the condition illustrated in Fig. 7 and formulated in (21) is satisfied. Also, both plots indicate that the bore through which the inner conductor passes should not have the cylindrical shape as it was assumed for volume calculations. Rather, its shape should be tapered so that the SucoPearl contacts the inner conductor along the smallest bore circumference, or the contact line. Plot (*a*) in Fig. 9 shows the version where the contact line is placed at the mid-surface, and Plot (*b*) shows the second version with contact line at the inner SucoPearl surface. This version is described by redefining the angle α_C in (16) to

$$\alpha_C = \frac{\Delta_{SP} + r_I}{R_N}. \tag{25}$$

Note that both eccentricity e and average strain $\bar{\varepsilon}$ along the bent centerline are significantly smaller if the

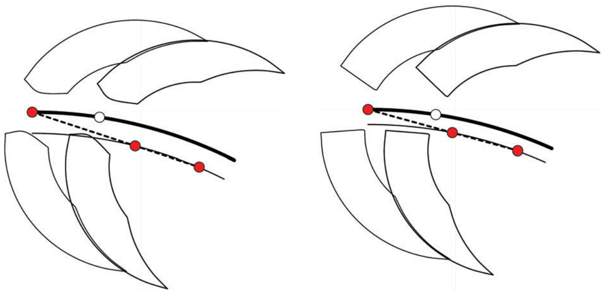

a) $\varepsilon = 505\mu,\ \bar{e} = -5.0\%$ b) $\varepsilon = 355\mu,\ \bar{e} = -3.6\%$

Figure 9 Kinematic theory applied to $r_O = 3$, $r_I = 2$, $r_{IC} = 0.5$, $\varphi = 75$, $r_n = 20$. Sucopearl attached to inner conductor at midplane (a) or at inner sphere radius (b).

SucoPearl is supported at the inner surface.
The necessary degree of tapering is dictated by the intended maximum bending curvature, or minimum bending radius. If the support is at the sphere's midplane, the bore is widened equally at the inner and outer surfaces as can be seen in Fig. 9a). The widening depends on the relative rotation between the SucoPearl and the inner conductor,

$$\alpha_{rel} = \alpha_C \left(1 + \frac{r_O - r_M}{R_N}\right) - \frac{\alpha_B}{2} \tag{26}$$

where the second term in parentheses considers the change of angle along the curved inner-conductor center line. The tapering is then described by the widening factor

$$f_{taper} = 1 + 2tan(\alpha_{rel})\,(r_O - r_M)\ . \tag{27}$$

If the support is at the sphere's inner surface, the bore is widened at the outer surface only as can be seen in Fig. 9b). Then, the relative rotation between the SucoPearl and the inner conductor becomes,

$$\alpha_{rel} = \alpha_C \left(1 + \frac{r_O - r_I}{R_N}\right) - \frac{\alpha_B}{2} \tag{28}$$

and the tapering is described by the widening factor

$$f_{taper} = 1 + 2tan\,\alpha_{rel}\,(r_O - r_I)\ . \tag{29}$$

The line of contact, ring-shaped in the reference configuration, will become an ellipse due to the rotation of the SucoPearl with respect to the inner-conductor. The elongation $\varepsilon_{\bigcirc}$ of the contact ring is approximately described by:

$$\varepsilon_{\bigcirc} = \frac{1}{cos\left(\alpha_C - \dfrac{\alpha_B}{2}\right)}\ . \tag{30}$$

4 Results for relevant geometries and bending

4.1 Geometric parameter study

The study is conducted on two geometric SucoPearl versions, namely *SP304* and *SP306* given in Table 1. Bore and sphere outer surface radii agree with dielectric radii of existing co-axial cables [4]. We consider

Table 1 Geometries of *SP304* and *SP306*

	$R_I[mm]$	$R_O[mm]$	$R_{CI}[mm]$
SP304	1.730	1.930	0.815
SP306	2.525	2.825	1.190

the influence of the opening angle φ on geometric properties where the shapes are illustrated in Fig. 10. The geometries of the two SucoPearl types are shown with identical scaling to give a visual impression of the relative size. The geometric parameter ratios of both types are very similar, which is observable from nearly identical values of volume fraction and limit rotation. Impractical designs are found with very small ($\varphi = 31°$) and large ($\varphi = 86°$) opening angles: The design with $\varphi = 31°$ will create straight lines of unshielded view between inner and outer conductors at small relative SucoPearl rotations whereas the other design with $\varphi = 86°$ provides no mass advantage over solid dielectrics as it fills all of the space with material. The values shown in Fig. 10 are used for the illustrative plots in Fig. 11 and 12: Fig. 11 contains the plot of the periodic spacing Δ_{SP}. It must be noted that the number of needed SucoPearls increases with decreasing periodic spacing. Fig. 12 contains the plot of the volume fraction v_f versus the opening angle φ. It can be seen that the desired advantage of the SucoPearl design, namely to save mass with respect to solid-dielectric designs, vanishes as the opening angle approaches its upper limit.

4.2 Kinematic results of the parameter study

All geometric versions are subjected to bending that is measured in terms of the nominal inner-conductor bending radius R_N. As eccentricity of the outer conductor with respect to the inner conductor is critical for the electric performance, the bending radii are adjusted for each design to create the tolerated eccentricities $e_{crit}^{(SP304)} = 40\mu$ and $e_{crit}^{(SP306)} = 70\mu$, respectively. The results are listed in Table 2 and visualized by the plots in Fig. 13. It can be seen that limit bending radii decrease with increasing opening angle and that supporting the SucoPearls at their inner sphere surface allows for smaller radii than supporting them at the sphere's midplane.
Table 3 shows that axial compressive strain, kinematically enforced by bending kinematics under the assumption that the inner conductor be much stiffer than other cable components, increases with opening angles. The larger design version *SP306* suffers higher strains than the smaller version *SP304*, and the support at the inner sphere surface lead to higher strains than the other support. Fig. 14 visualizes the data of Table 3. Because of the rotation of SucoPearls on the inner conductor the contact line cannot remain circular.

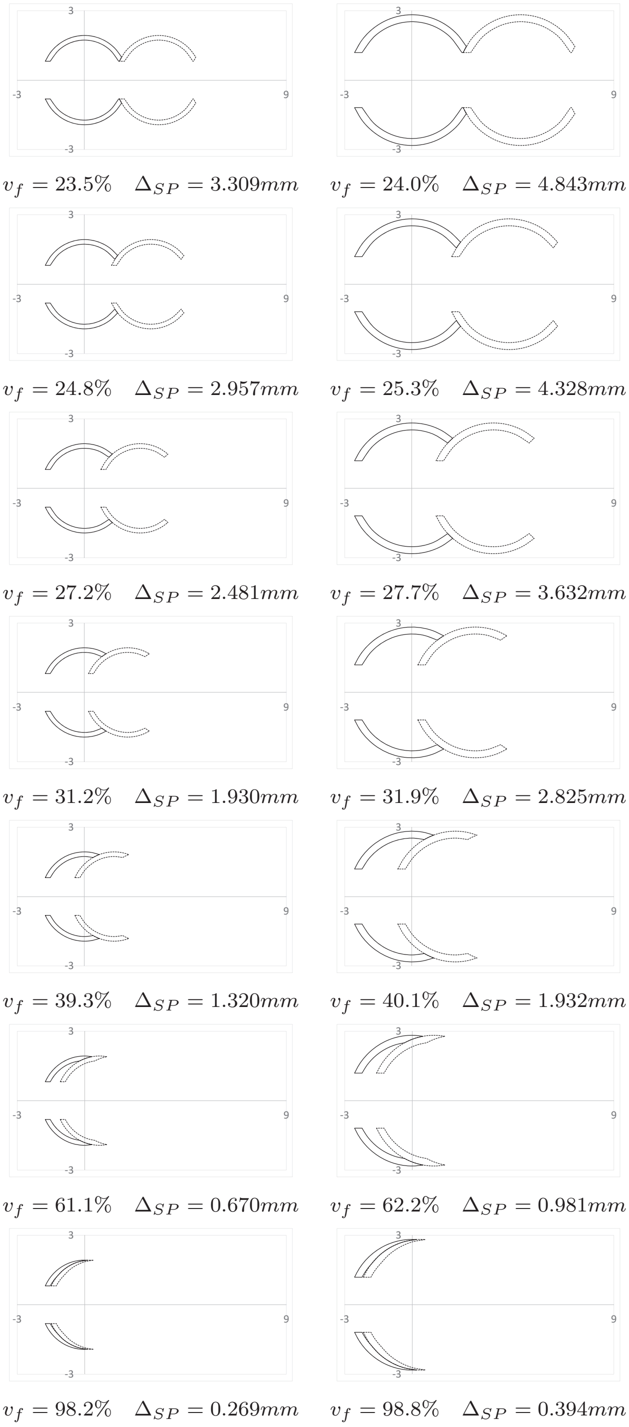

Figure 10 SucoPearl shapes, volume fractions, and limit rotations. Opening angles φ from top to bottom: 31°, 40°, 50°, 60°, 70°, 80°, 86°.

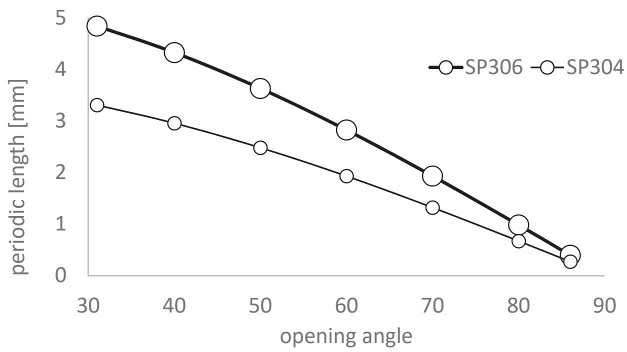

Figure 11 Periodic spacing Δ_{SP} versus opening angle φ

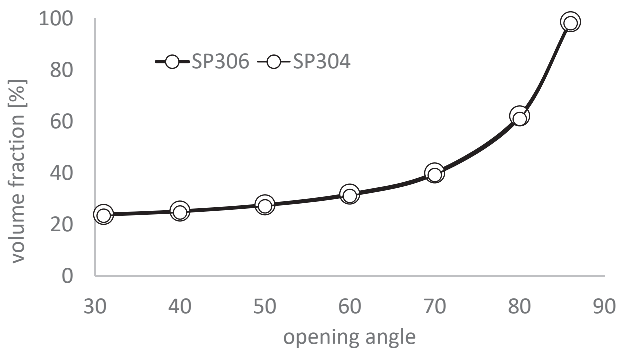

Figure 12 Volume fraction v_f versus opening angle φ

Table 2 Bending radii $R_N[mm]$ for maximum tolerated eccentricities. Superscripts refer to positions of contact lines to inner conductor.

	SP304		SP306	
φ	$R_{lim}^{(1)}$	$R_{lim}^{(2)}$	$R_{lim}^{(1)}$	$R_{lim}^{(2)}$
31	117.6	109.0	143.8	133.0
40	109.6	101.4	133.9	123.7
50	98.7	91.1	120.6	111.1
60	86.1	79.2	105.2	96.6
70	72.1	66.0	88.1	80.4
80	57.2	51.9	69.9	63.3
86	48.1	43.3	58.7	52.7

Rather, the one axis remains constants whereas the other axis must become longer. The elongation is expressed in terms of strain. Table 4 lists the values and Fig. 15 visualizes them. Except for the sign, the trends observed from this table are similar to those of the averaged axial strains. It can be concluded that, at the respective limit bending radii, the larger SucoPearls *SP306* suffer higher strains than the smaller *SP304*. Within the interesting range of opening angles, say $40° \leq \varphi \leq 60°$, all average strains do not exceed 0.1%.

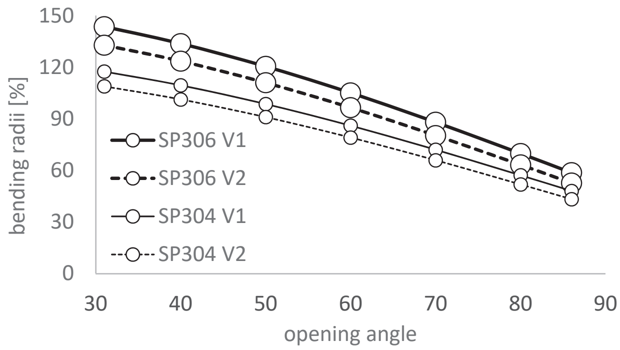

Figure 13 Limit bending radii R_N versus opening angle φ. The limits refer to tolerated eccentricities $e = 40\mu$ and $e = 70\mu$ for the types SP304 and SP306, respectively.

Table 3 Axial strains $\bar{\varepsilon}_{axial}[\%]$ for maximum tolerated eccentricities. Superscripts refer to positions of contact lines to inner conductor.

	SP304		SP306	
φ	$\bar{\varepsilon}^{(1)}_{axial}$	$\bar{\varepsilon}^{(2)}_{axial}$	$\bar{\varepsilon}^{(1)}_{axial}$	$\bar{\varepsilon}^{(2)}_{axial}$
31	−0.0340	−0.0367	−0.0486	−0.0526
40	−0.0365	−0.0394	−0.0523	−0.0566
50	−0.0405	−0.0439	−0.0580	−0.0630
60	−0.0464	−0.0505	−0.0665	−0.0724
70	−0.0555	−0.0606	−0.0794	−0.0871
80	−0.0699	−0.0770	−0.1000	−0.1105
86	−0.0830	−0.0922	−0.1191	−0.1327

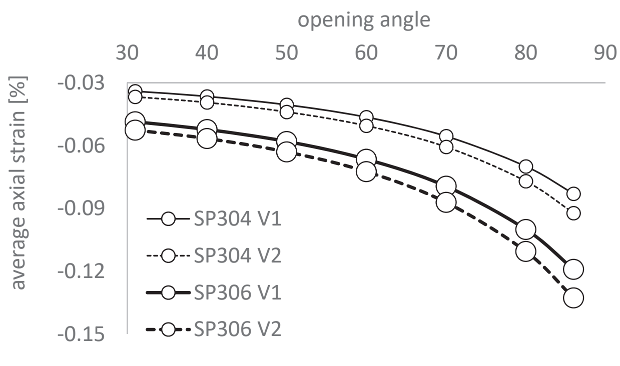

Figure 14 Average axial strain $\bar{\varepsilon}_{axial}$ versus opening angle φ.

5 Critical discussion

5.1 Basic performance properties

The model assumptions are justified by the current cable design, where the stiffness values of the outer conductor and jacket materials are so small that their interaction

Table 4 Deviation $\varepsilon_{\bigcirc}[\%]$ away from a circular shape to an ellipse of contact lines. Superscripts refer to positions of contact lines to inner conductor.

	SP304		SP306	
φ	$\varepsilon^{(1)}_{\bigcirc}$	$\varepsilon^{(2)}_{\bigcirc}$	$\varepsilon^{(1)}_{\bigcirc}$	$\varepsilon^{(2)}_{\bigcirc}$
31	0.0439	0.0482	0.0628	0.0692
40	0.0456	0.0500	0.0653	0.0719
50	0.0484	0.0532	0.0694	0.0764
60	0.0527	0.0579	0.0755	0.0831
70	0.0597	0.0665	0.0855	0.0944
80	0.0717	0.0792	0.11026	0.1136
86	0.0835	0.0928	0.1198	0.1335

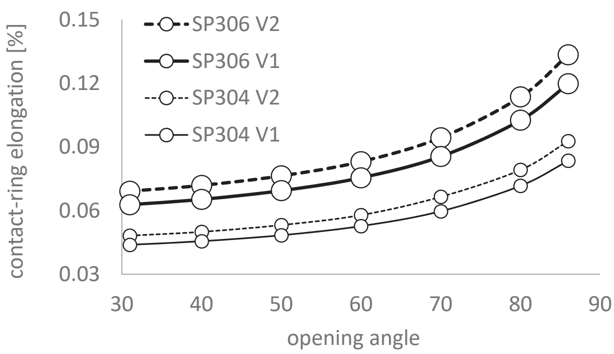

Figure 15 Contact-ring elongation $\varepsilon_{\bigcirc}$ versus opening angle φ.

with the SucoPearl does not have much influence on the deformation of the latter. The cables can be bent to a radius almost as small as ten times the cable diameter if the SucoPearls are rather short. If the SucoPearls are desired to be longer, the minimum radii are restricted to be somewhat larger. In any case, the study shows that the SucoPearl concept is feasible as the eccentricity due to bending is kinematically controlled and will stay within the required limits. From a practical point-of-view, the advantage of the SucoPearl design, namely mass saving, is quite significant in view of launching cost for satellites. On the other hand, eccentricity due to layout bending is higher than with solid dielectric design.

5.2 Mass and eccentricity: Conflict of objectives

Dielectric-mass reduction of co-axial radio-frequency cables for space applications is the driving motivation of this research. Apart from the size dictated by the outer diameter of the inner conductor and the inner diameter of the outer conductor, the SucoPearl wall thickness and the opening angle φ remain as design parameters. The latter provokes a conflict of objectives: Smallest values of φ promise the highest mass reduction but restrict the bending to large radii that might be impracticable when it comes to laying cables within a satellite. As the bending is restricted by tolerated values of eccentricity, it is interesting to compare the SucoPearl-design with solid dielectric designs, where bending-driven eccentricity is traced back to the transverse-strain effect. Teflon, a material often used for space applications, has a Poisson-ratio value of about $\nu = 0.46$. Fig. 16 illustrates a much simplified model assumption

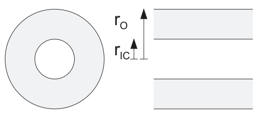

Figure 16 Illustration of simplified substitute model for estimating transverse-strain effect in co-axial cable

for estimating eccentricity in a coaxial cable by a laminated-plate analogy. The shaded areas in the figure indicate the dielectric material whereas the white areas stand for the inner-conductor material. Under cylindrical bending, the absolute though-thickness displacement of the outer-layer surfaces is given by

$$\begin{aligned} e_{solid} &= -\frac{1}{R_N}\left(\int_0^{r_{IC}} \nu_{IC} z dz + \int_{r_{IC}}^{r_O} \nu_{DE} z dz\right) \\ &= -\frac{1}{2R_N}\left(r_{IC}^2 \nu_{IC} + \left(r_O^2 - r_{IC}^2\right)\nu_{DE}\right) \end{aligned} \quad . \quad (31)$$

We use this result to roughly estimate the eccentricity of the cable. Fig. 17 shows the eccentricities of the cables with solid-Teflon dielectric design at the same nominal bending radii R_N at which the respective SucoPearls designs experience their limit eccentricities. Versions 1 and 2 refer to the bore shapes (a) and (b)

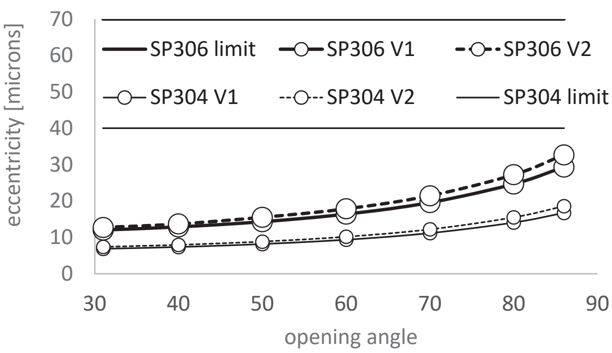

Figure 17 Comparison of estimated eccentricities: solid-Teflon designs are represented by marked lines. The SucoPearl limit eccentricities are indicated by horizontal unmarked lines.

illustrated in Fig. 9, respectively. The solid-dielectric-design eccentricities are always significantly smaller than those of the SucoPearl designs indicated with the horizontal lines. The SucoPearl-design advantage of mass savings is in conflict with its limitations regarding bending, or layout flexibility.

5.3 Axial strain and the risk of damage

The strength of the model lies in its simplicity. The simplifying assumptions include that the averaged strains along the curved lines of inner and outer conductor must be different and the model does not answer the question how the mismatch of the averaged strains translates into local deformations and strains of the cable constituents. The question touches the problem of material strength and answers can be found by applying the theory of elasticity with the help of numerical analysis with the finite-element method (FEM).

5.4 Manufacturing

The SucoPearl shape with proposed constant shell thickness and undercut poses a manufacturing challenge.

6 Conclusion and outlook

A closed-form exact model for analyzing the kinematic behavior of a co-axial cable with a periodic dielectric structure consisting of a chain of pearls has been developed and the cable design analyzed. The overall conclusion is that the SucoPearl design is feasible as the eccentricity due to bending can be kinematically controlled and will stay within the required specifications. A critical discussion followed from the analysis and addressed the problem that the remaining question of an average strain mismatch, causing local strains in all cable constituents, requires a theory-of-elasticity approach. The elastic analysis of the present problem will be considered in the near future. An opportunity for better model verification will be provided by comparing the predictions of the closed-form kinematic and the numerical elasticity models.

Nomenclature

e	eccentricity of conductors due to bending
e_{solid}	eccentricity of conductors with solid dielectric
f_{taper}	widening factor to describe bore tapering
m_f	mass fraction of sucopearl to cylindric dielectric
r_{cont}	sucopearl-contact point radial position
r_I	sucopearl inner surface radius
r_{IC}	inner-conductor radius
r_M	sucopearl mid-surface radius
r_O	sucopearl outer surface radius
v_f	volume fraction of sucopearl to cylindric dielectric
x, y	reference system coordinates

x_{cont} sucopearl-contact point axial position

A, B center points of adjacent sucopearls

C point at inner conductor and sucopearl contact

L_{SP} sucopearl length

N_{SP} number of sucopearls per periodic length Δ

N_{SP} number of sucopearls per periodic length Δ

R_{CP} bending radius of sucopearl center line

R_{lim} limit bending radius for preserving shielding

R_N bending radius of inner-conductor center line

V_{cyl} cylindric dielectric volume over sucopearl length

V_{SP} sucopearl volume

α_B angular position of point B in bent configuration

α_C angular position of point C in bent configuration

α_{lim} limit angle for preserving shielding

α_{rel} rotation of sucopearl against inner conductor

$\bar{\varepsilon}$ axial deformation discrepancy per unit length

$\varepsilon_{\bigcirc}$ elongation of contacting circle due to bending

φ opening angle

φ_{max} maximum opening angle

ν_{DE} Poisson's ratio of solid dielectric material

ν_{IC} Poisson's ratio of inner-conductor material

ρ_{cyl} sucopearl-material mass density

ρ_{SP} cylindric dielectric mass density

θ angle variable about axial direction

Δ_L sucopearl spacing or periodic length

Δ_{SP} sucopearl spacing or periodic length

Acknowledgements

The authors gratefully acknowledge the support of the ESA-ARTES-5 Programme, Project *Lightweight RF Power Cable with High Phase Stability*, ESTEC Contract No. 22589/09/NL/GLC. The present model has been developed out of the necessity of predicting co-axial-cable internal eccentricity under bending, and the authors would like to thank the project team members for the good collaboration as well as fruitful and inspiring discussions, namely: Kuno Wettstein, Stefan Metz, Eden Sorolla, Michael Rupflin, Josef Fuchs, and Ioannis Koufogiannis.

References

[1] Rodney, J. and Vaughan, M. (1988) 'Multipactor', *IEEE Trans. Electron Devices*, Vol. 35, No. 7, pp.1172–1180

[2] Wikipedia, 'Multipactor effect', http://en.wikipedia.org/wiki/Multipactor_effect

[3] Spergel, J. (1972) 'Coaxial cable and connector systems, in: C.A. Harper (Ed.), *Handbook of Wiring, Cabling, and Interconnecting for Electronics, McGraw-Hill, New York, N.Y., 1972*

[4] Huber+Suhner AG, Degersheimerstrasse 14, CH-9100 Herisau, Switzerland

[5] Karstensen, H., Koufogiannis, I., Sorolla, E., Kress, G., Mattes, M., Rupflin, M., Fuches, J., Wettstein, K. (2013) 'Phase stable RF cable for space applications', *Space Passive Component Days, 1st International Symposium, ESA/ESTEC*, Noordwijk, The Netherlands, 24-26 September

[6] Karstensen, H., Koufogiannis, I., Sorolla, E., Kress, G., Mattes, M., Rupflin, M., Fuches, J., Wettstein, K., Raboso, D. (2014) 'Extremely phase stable RF cable for space applications', *Mulcocim 2014*, Valencia, Spain, 17-20 September